IEEE Access
Multidisciplinary ⋮ Rapid Review ⋮ Open Access Journal

Received 13 December 2022, accepted 29 December 2022, date of publication 30 December 2022,
date of current version 5 January 2023.

Digital Object Identifier 10.1109/ACCESS.2022.3233471

RESEARCH ARTICLE

A Curved Microstrip Patch Antenna Designed From Transparent Conductive Films

GIORGIO MONTISCI[1], (Senior Member, IEEE), GIOVANNA MURA[1], (Member, IEEE), GIACOMO MUNTONI[1], GIOVANNI ANDREA CASULA[1], (Senior Member, IEEE), FRANCESCO PAOLO CHIETERA[2], AND MAHMOUD ABURISH-HMIDAT[3]

[1]Dipartimento di Ingegneria Elettrica ed Elettronica, Università degli Studi di Cagliari, 09123 Cagliari, Italy
[2]Dipartimento di Ingegneria dell'Innovazione, Università del Salento, 73100 Lecce, Italy
[3]FILAR Optomaterials, 08048 Tortolì, Italy

Corresponding author: Giorgio Montisci (giorgio.montisci@unica.it)

This work was supported in part by the Fondazione di Sardegna through the project ARGOSAT–Microsatellite Cluster for the Observation of Optical Transients in Astronomy under Grant CUP:F74I19001070007.

ABSTRACT Transparent microstrip patch antennas suffer from low radiation efficiency and gain when manufactured using transparent conductive films (TCFs), mainly at low frequency (starting from the microwave S band). To address this problem, we propose a curved microstrip patch antenna designed using transparent materials. This new configuration has proven to be a simple and effective solution to improve the radiation efficiency and gain of TCF printed antennas. In fact, when typical values of the TCF surface resistance are considered (between 2 and 10 Ω/sq), the new antenna features a radiation efficiency of up to 72.3% and a realized gain of up to 5.3 dBi at 2.15 GHz, with a significant improvement in comparison with the flat transparent microstrip antenna (up to 17.7% radiation efficiency, and 0.5 dBi realized gain). Good transparency and lightweight is ensured by the deposition of the TCF on a polyethylene terephthalate film, which lies, in turn, on a 3D-printed curved polyethylene terephthalate glycol supporting frame. Simulations using Ansys HFSS are presented to demonstrate the potential of the proposed configuration. Then, a prototype of the transparent curved patch antenna is fabricated and measured to assess the simulated results.

INDEX TERMS Curved microstrip antenna, microstrip antennas, transparent antennas, transparent conductive films.

I. INTRODUCTION

Antennas made of transparent conductive parts have attracted increasing attention in the recent years [1], mainly for solar panel applications. In this context, conductors are generally implemented in two forms: using conductive meshes [2], [3], [4], [5], [6] or by means of transparent conductive films (TCFs) [7], [8], [9], [10], [11], [12], [13], [14]. Meshed antennas generally ensure good transparency and electromagnetic performance. However, the grid width (or line width of the mesh) is the main problem since it should be optimized to find a compromise between optical transparency and electromagnetic performance [5]. An alternative solution for the implementation of the antenna conductors relies on TCFs. They are fabricated using different materials, mostly based on indium tin oxide (ITO) [7], [9], [10], [12], [13], fluorine-doped tin oxide [7], and silver coated polyester films (AgHT) [8], [11]. Multilayer films have also been used recently [14]. These TCFs are deposited on suitable substrates, such as glass or plastic (e.g., polyethylene terephthalate (PET)), typically using sputter deposition [15]. Unfortunately, the performance of antennas realized using this technology is generally poor due to the high losses of the conductors. As a matter of fact, economic TCFs exhibit surface resistance typically between 2 and 10 Ω/sq [1], [7], [8], [9], [10], [11], [12], [13], [14], also depending on the thickness of the TCF deposition. A thicker coating layer would reduce the surface resistance but at the expense of increased manufacturing cost and reduced transparency.

Viable solutions using TCFs include the realization of reflectarray antennas (e.g., in [12], operating at 26 GHz) or aperture coupled antennas (in [13], at 10 GHz) that, despite

The associate editor coordinating the review of this manuscript and approving it for publication was Ladislau Matekovits.

the complicated design and realization, have proven to be less sensitive to the high surface resistance of the TCFs. However, it is important to observe that the skin depth is inversely proportional to the square root of the frequency. In contrast, the conductivity of the TCFs does not vary significantly with frequency (see e.g. [16], up to 20 GHz). Therefore, ohmic losses of antennas manufactured using TCFs increase substantially when the operating frequency decreases. In particular, the radiation efficiency reduction of TCF patch antennas becomes critical in the lower part of the S band, i.e., around 2.5 GHz or lower [9]. In the following, we will focus on patch antennas operating at those frequencies.

In [8], a method for improving the efficiency of TCF coplanar waveguide (CPW) patch antennas at 2.2 GHz is proposed by applying a highly conductive metallization at the edges of the CPW slots, reaching an efficiency of 68% at the cost of a small reduction of the transparency. However, this configuration presents high back radiation, with two equal gain peaks at 0° and 180° and might not be the best solution for solar panel applications.

On the other hand, TCF microstrip patch antennas suffer from very low radiation efficiency, as shown in [9] where an ITO (90% optically transparent) patch antenna on a copper ground plane exhibits a radiation efficiency of 15% at 2.5 GHz. In [9] and [10] it is also shown that the efficiency of microstrip patch antennas with TCF metallic parts dramatically drops when the operating frequency reduces. In [14], a 5μm-thick metal mesh copper film is used to fabricate a standard microstrip patch antenna at 2.45 GHz. Although this TCF exhibits a surface resistance as low as 0.18 Ω/sq, the proposed antenna features just acceptable radiation efficiency and gain (43% and 2.63 dBi, respectively) and 62% transparency. A patch antenna using an IZTO/Ag/IZTO film with a surface resistance of 2.52 Ω/sq is also designed in [14], but its efficiency is only 8% and the gain is −4.2 dBi.

Transparent meshed antennas generally provide higher radiation efficiency in the S band than TCF patch antennas. In [3], a feasibility study of integrating optically transparent meshed patch antennas on the top of off-the-shelf solar cells is presented. Ink-meshed and wire-meshed patches at 2.5 GHz have been manufactured achieving a transparency of 61% and 93%, respectively. Unfortunately, in [3] the authors do not report the gain and the efficiency of the manufactured prototypes. In [6], a silver epoxy meshed patch antenna is proposed at 2.4 GHz, featuring excellent transparency (higher than 90%) and good electromagnetic performance (gain equal to 4.94 dBi), though also in this case the radiation efficiency is not computed. In [5], a parametric analysis of meshed patch antennas on a copper ground plane is presented at around 2.0 GHz. It is shown that, for a grid width equal to 1 mm, a meshed patch with 60% transparency yields a radiation efficiency of 77% and a gain of 6.3 dBi, whereas a meshed patch with 80% transparency features a radiation efficiency of 55% and a gain of 4.1 dBi.

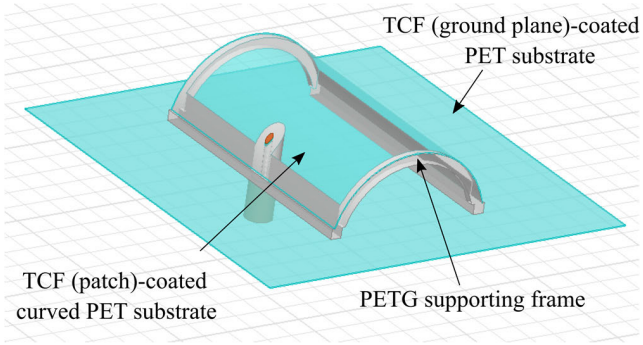

FIGURE 1. 3D view of the proposed TCF curved patch antenna.

Finally, in [17], a direct comparative study of the performance of transparent patch antennas fabricated using either conductive meshes or TCFs is performed at 2.5 GHz. It is shown that meshed antennas exhibit a better electromagnetic performance than TCF antennas. Specifically, a meshed antenna with 90% transparency features a radiation efficiency of 61%, whereas an ITO patch antenna with 90% transparency provides a very poor radiation efficiency (less than 15%).

Aiming to improve the efficiency and gain of TCF microstrip patch antennas, in this paper, we propose a modified version of the curved microstrip patch antenna presented by some of the authors in [18], which has been designed here at the center frequency of 2.15 GHz to comply with the specifications of antennas for solar panel applications (Fig. 1).

The antenna in [18] is manufactured at 2.45 GHz using a 3D-printed Polylactic Acid (PLA) curved substrate (dielectric permittivity 2.54, $\tan\delta = 0.015$) with a 35μm-thick adhesive copper tape employed to realize the ground plane and the curved patch. That configuration ensures an improved percentage bandwidth compared with its flat counterpart, i.e., 9.3% (against 3.3%) and a reduction of the projected antenna resonant size of up to 38%.

A TCF curved patch antenna (TCPA) can be designed by suitably modifying the materials employed in [18]. In this regard, using a TCF in place of the copper tape and a transparent dielectric material in place of the PLA may seem a trivial solution to the problem of the TCPA design. However, this is not entirely true since the reduced conductivity of the TCFs invalidates most of the results presented in [18], wherein a good conductor (i.e., copper) is used. As a consequence, an accurate analysis is required to properly characterize the new TCPA and highlight the improvements achievable in comparison with the TCF flat microstrip antenna. Moreover, since transparent antennas are important in cubesat and satellite applications [19], the new design proposed here should address two important points:

1) A quite large frequency bandwidth could be necessary for space applications as, for example, when the antenna needs to be used in the S frequency band for

TABLE 1. Performance comparison of S band transparent patch antennas.

	Operating Frequency (GHz)	Patch Conductor	Surface resistance (Ω/sq)	Radiation efficiency (%)	Transparency (%)	Gain (dBi)	Method for computing/ measuring transparency	Ground plane
Meshed-1 [5]	~ 2.0	Copper wire mesh	-	77 (simulated)	60	6.3 (simulated)	Percentage of see-through area of the patch [5]	Solid conductor (microstrip)
Meshed-2 [5]	~ 2.0	Copper wire mesh	-	55 (simulated)	80	4.1 (simulated)	Percentage of see-through area of the patch [5]	Solid conductor (microstrip)
Meshed-3 [17]	2.5	Copper wire mesh		61 (simulated)	90	Not computed	Percentage of see-through area of the patch [5]	Solid copper (microstrip)
Meshed-4 [3]	2.5	Copper wire mesh	-	Not computed	93	Not computed	Percentage of see-through area of the patch [5]	Solid conductor (microstrip)
Meshed-5 [3]	2.5	Conductive ink mesh	-	Not computed	61	Not computed	Percentage of see-through area of the patch [5]	Solid conductor (microstrip)
Meshed-6 [6]	2.4	Silver epoxy mesh	-	Not computed	> 90	5	Percentage of see-through area of the antenna	Same as patch (microstrip)
TCF-CPW [8]	2.2	AgHT-4 film	4.5	68 (simulated)	Not computed	Not computed	-	Same as patch (CPW)
TCF-1 [14]	2.5	Copper-mesh film	0.18	42.7	62	2.63	Average value based on spectrometer measurements	Same as patch (microstrip)
TCF-2 [14]	2.5	IZTO/Ag/IZTO film	2.52	7.8	69	-4.23	Average value based on spectrometer measurements	Same as patch (microstrip)
TCF-3 [17]	2.5	ITO	4.6	15 (simulated)	90	Not computed	Equation (1) of [9]	Solid copper (microstrip)
TCF-4 [9]	2.5	ITO	~ 4	< 15 (simulated)	90	Not computed	Equation (1) of [9]	Solid copper (microstrip)
This work (flat)	2.15	TCF (generic)	from 2 to 4	from 9 to 18 (simulated)	-	from -2.7 to 0.5 (simulated)	-	Same as patch (microstrip)
This work (curved)	2.15	TCF (generic)	from 2 to 8	from 41 to 72 (simulated)	-	from 2.5 to 5.3 (simulated)	-	Same as patch (microstrip)
This work (curved prototype)	2.15	In2O3/Au/Ag	between 7 and 8	between 41 and 44 (simulated)	71	2.57	Ratio of the output powers of a solar panel [13, 22]	Same as patch (microstrip)

Telemetry, Tracking and Command applications (i.e., from 2.025 GHz to 2.29 GHz). The TCPA presented here features an improved bandwidth compared both with the TCF flat microstrip antenna and with the curved antenna proposed in [18]. The bandwidth enhancement is due to two combined factors: the curved configuration (as pointed out in [18]) and the lower conductivity of the TCFs compared with copper. Specifically, the low conductivity of the TCFs is an important drawback, since it increases ohmic losses, reducing the antenna efficiency. However, this effect is less critical in the curved configuration, since the radiation quality factor of the curved microstrip antenna is lower than that of the standard flat microstrip antenna [18].

2) The weight reduction of the electronic payload is a critical task in space applications. The weight of the antenna proposed in [18] (scaled at 2.15 GHz) is 26 g, whereas with the modified design presented here, the antenna weight reduces to 5 g. This is achieved using a thin polyethylene terephthalate glycol (PETG) frame supporting a curved TCF-coated 0.2 mm thick PET layer (Fig. 1) with the additional benefit of reducing overall dielectric losses.

In section II, we present the TCPA geometry and we analyze its performance compared with the flat counterpart. All the simulations have been performed using Ansys HFSS, a reliable commercial software for the solution of electromagnetic problems, whose simulated results are in excellent agreement with measurements (see. e.g. [20], [21]). In the HFSS simulations, the surface resistance of the TCFs has been set between 0.01 Ω/sq and 10 Ω/sq with a center frequency of 2.15 GHz. The advantages, in terms of radiation efficiency, of the TCPA proposed here over the TCF flat microstrip antenna, will be clearly highlighted in section II. In particular, the TCPA exhibits a radiation efficiency of up

to 72.3% (for surface resistance ≥ 2 Ω/sq), with an increase by at least a factor of 4 over the transparent flat counterpart. To make a comparison, the curved patch antenna in [18] provides an increase by a factor of only 1.3 (from 67% of the flat microstrip antenna to 86% of the curved one).

To summarize the contribution of our work in the light of the state of the art, the performance of transparent microstrip patch antennas selected from the literature, operating in the S band (around 2.5 GHz or lower), is reported in Table 1. This comparison clearly shows the improved radiation efficiency of the TCPA proposed in this work over the TCF flat patch antenna. Moreover, it can be seen that the curved configuration is able to fill the radiation efficiency gap between TCF antennas and meshed antennas in the lower part of the S band.

For a consistent comparison, it should be noted that the patch antennas proposed in [3], [5], [9], and [17] (included in the comparison of Table 1), employ good conductors for the ground plane, since a solar cell is intended as a part of the antenna substrate and provides, with its back-side, the metallic ground plane, usually made of copper [9], gold [3], and silver [12], [13], [22]. This solution allows improved radiation efficiency thanks to the ground plane made of a good conductor, and better transparency since it requires only one layer of TCF/meshed-conductors on the surface of the solar cell exposed to the light. In this context, also the curved configuration proposed in this work could be integrated into a solar cell that provides the metallic ground plane. Though this analysis is beyond the scope of this work, it is clear that, also in this case, the transparent curved patch will maintain its advantages over the transparent flat patch in terms of radiation efficiency and gain.

To validate the performance of the proposed solution, a prototype of the curved antenna has been manufactured and measured, delivering good optical transparency (about 70%) and lightweight (5 g including the SMA connector). The materials employed for prototyping are described and characterized in Section III. Specifically, we have used a commercial PET substrate with an In_2O_3/Au/Ag transparent conductive coating for the patch antenna and its ground plane, and 3D-printed PETG to manufacture the dielectric frame supporting the curved TCF-coated PET film (see Fig. 1).

II. ANTENNA DESIGN AND SIMULATIONS

The antenna geometry is shown in Figs. 1 and 2. A dielectric (PETG in our case) curved frame of thickness $H_S = 2$ mm and height H_B supports a 0.2 mm-thick curved PET film coated with a TCF in the upper side, i.e., the patch antenna. The width of the patch is W, the radius of curvature of the PET film is equal to R_H, and the projected planar resonant size of the patch is L. The antenna ground plane is provided by the same TCF deposited on a 0.2 mm-thick PET film (see Figs. 1 and 2). The spacing between the PET film at the bottom and the curved supporting frame is provided by two PETG square cuboids with base $H_S \times H_S$ and height W. A horizontal offset $dx = 0.5$ mm (see Fig. 2b) between the

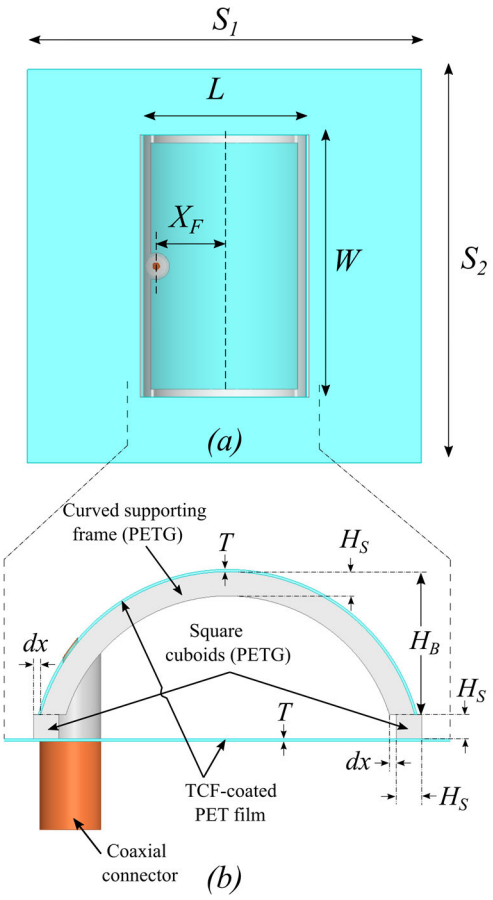

FIGURE 2. Geometry of the curved antenna: top view (a), magnified side view (b).

curved frame and the base cuboids is employed to improve the adherence of the PET film to the curved PETG supporting frame.

The dielectric permittivity of both PET and PETG is 2.5 with loss tangent 0.01. The substrate extension $S_1 = S_2$ (see Fig. 2a) is set to 75 mm and the width W of the patch is equal to 50 mm.

As pointed out in [18], the first step of the antenna design is the selection of the bending radius R_H, which is set here to 16 mm. Then L and, consequently, the corresponding value of H_B (see Fig. 2b) are chosen to get the resonance at 2.15 GHz. Finally, the position of the coaxial connector X_F is selected to match the antenna to the 50 Ω coaxial connector.

In this section, we analyze the performance of the TCPA for different values of the TCF surface resistance R_S. Then, to demonstrate the capability of this configuration to achieve good radiation efficiency and gain even when the metallization exhibits relatively high values of R_S, we compare its electromagnetic behavior with that of the standard flat patch antenna. The latter is obtained with the same geometry depicted in Fig. 2, for a bending radius $R_H = \infty$ and $S_1 = 90$ mm.

In Table 2, the geometrical parameters and the simulated electromagnetic performance (realized peak gain G_R, directivity Dir, radiation efficiency η, and bandwidth B) of the

TABLE 2. Geometrical parameters and simulated electromagnetic performance of the TCPA at 2.15 GHz, $H_S = 2$ mm, RL > 30 dB.

R_S (Ω/sq)	H_B (mm)	X_F (mm)	L (mm)	G_R (dBi)	Dir (dBi)	η (%)	B (MHz)
0.01	10.8	10.3	30.68	6.65	6.78	96.9	197
1	10.9	10.7	30.75	5.93	6.76	82.4	229
2	11.0	11.1	30.82	5.31	6.73	72.3	265
3	11.1	11.4	30.88	4.77	6.68	64.4	296
4	11.3	11.8	31.00	4.23	6.62	57.7	338
5	11.4	12.1	31.07	3.75	6.56	52.4	381
6	11.6	12.5	31.18	3.32	6.49	48.2	435
7	11.7	12.7	31.24	2.90	6.43	44.4	480
8	11.8	13	31.29	2.48	6.37	40.8	537
9	11.8	13	31.29	2.12	6.32	38.1	568
10	11.8	13	31.29	1.76	6.26	35.5	599

TABLE 3. Geometrical parameters and simulated electromagnetic performance of the transparent flat patch antenna at 2.15 GHz, $H_S = 2$ mm.

R_S (Ω/sq)	X_F (mm)	L (mm)	G_R (dBi)	D (dBi)	η (%)	RL (dB)	B (MHz)
0.01	8.75	56.9	7.6	8.12	88.5	> 30	42
1	15.9	57.2	2.8	8.08	29.6	> 30	125
1.5	18.5	57.2	1.5	8.03	22.0	> 30	164
2	21.3	57.2	0.5	8.00	17.7	> 30	208
3	26.0	57.3	-1.3	7.85	12.3	> 25	285
4	27.0	57.3	-2.7	7.73	9.3	> 17	322

curved antenna in Figs. 1 and 2 are summarized for different values of R_S. The same data pertaining to the flat antenna are reported in Table 3 for the comparison. It is worth noting that the latter cannot be matched (with return loss (RL) larger than 15 dB) for a surface resistance of the TCF larger than 4 Ω/sq, due to the prevalence of ohmic losses over the radiation conductance. The comparison between the results of Tables 2 and 3 shows that, for $R_S \geq 2$, the TCPA allows an improvement of the radiation efficiency by at least a factor of 4 over the TCF standard flat microstrip antenna and an improvement of the realized gain of more than 4.8 dBi.

It is also worth noting that the length L of the curved antenna is significantly reduced compared with the flat patch (from ∼57 mm to ∼31 mm), though at the expense of a lower directivity.

In Fig. 3, we report the return loss for selected values of R_S (only curved antenna) and, in Fig. 4, the realized gain G_R, showing the comparison between the frequency response of the TCPA and that of the flat counterpart. Finally, to summarize the results of Tables 2 and 3, in Fig. 5, we show a direct graphical comparison of the simulated realized gain and radiation efficiency of the curved and flat antennas at the center frequency of 2.15 GHz.

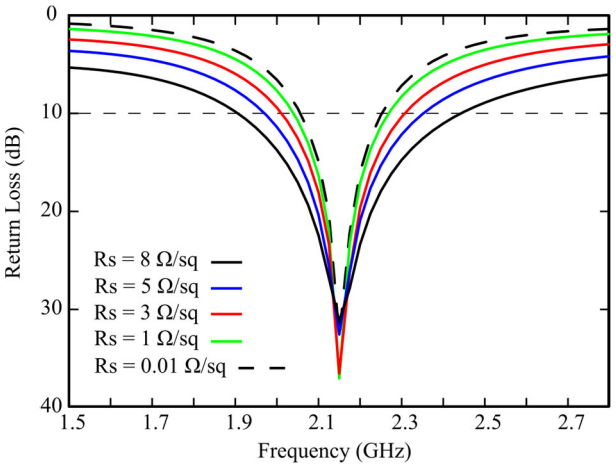

FIGURE 3. Simulated return loss (only curved antenna) for selected values of the surface resistance.

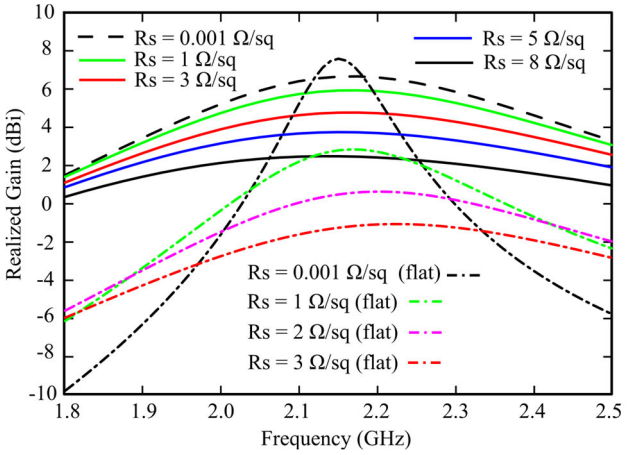

FIGURE 4. Simulated realized gain for selected values of the surface resistance. Comparison between the TCPA and the flat counterpart.

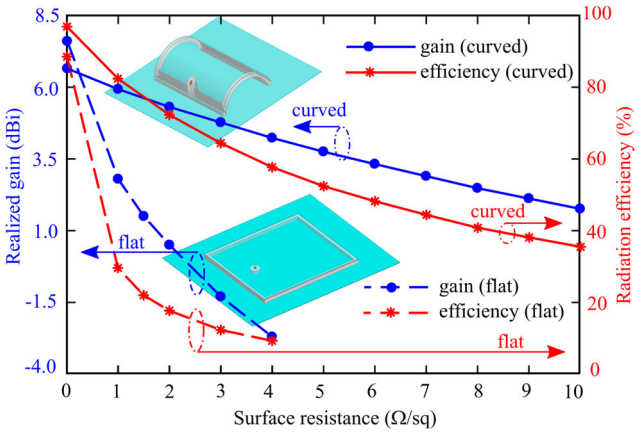

FIGURE 5. Simulated radiation efficiency and realized gain of the curved and flat transparent antennas at 2.15 GHz.

III. MATERIALS

In this section, we describe the materials employed for the experimental verification of the TCPA performance. Without loss of generality, any arbitrary TCF deposited on a transparent dielectric material could be suitable for this purpose. TCFs can be deposited on several materials, such as glass, polyethylene naphthalate (PEN), or PET. Among these, PET substrates are widely employed for the realization of planar antennas [13], [23] since they ensure low cost, lightweight, temperature stability, flexibility, chemical and

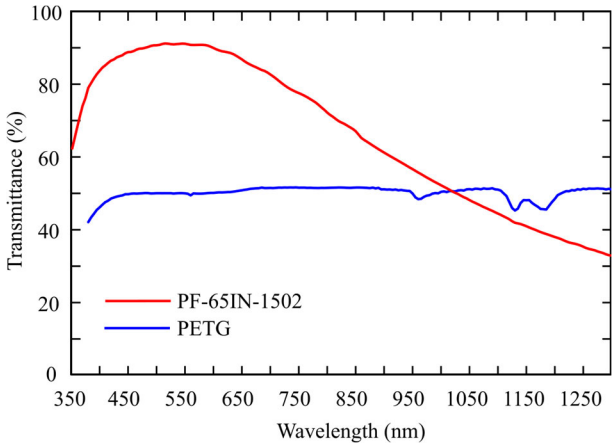

FIGURE 6. Transmittance of the 200μm PET film coated with In2O3/Au/Ag (part PF-65IN-1502 by Delta Technologies) and of the 2 mm-thick 3D-printed PETG substrate with 100% infill.

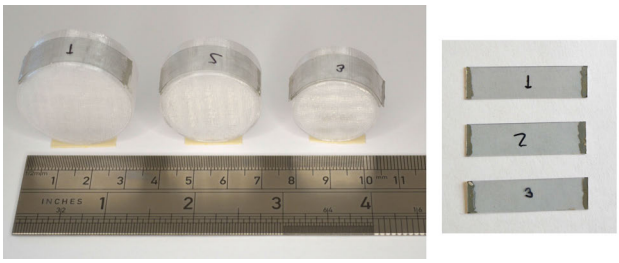

FIGURE 7. PF-65IN-1502 samples for the static measurement of the surface resistance: (left) curved with coating on the upper surface; (right) flat. Sample length = 35 mm, sample width = 10 mm.

TABLE 4. Surface resistance of different samples of the IN2O3/AU/AG coated PET film.

Type	Sample 1	Sample 2	Sample 3
Flat	9.1 Ω/sq	8.6 Ω/sq	8.6 Ω/sq
Curved (R_C = 17 mm)	9.2 Ω/sq		
Curved (R_C = 15 mm)		8.9 Ω/sq	
Curved (R_C = 13 mm)			12 Ω/sq

moisture resistance, durability, and a reasonable loss tangent, between 0.01 and 0.03, up to 10 GHz [24].

Unfortunately, it is not easy to find commercially available PET films with TCF coating featuring an arbitrary surface resistance. Moreover, the fabrication of tailored materials for specific applications requires specialized laboratories. In this work, we have selected a commercial In_2O_3/Au/Ag coated 0.2 mm-thick PET film by Delta Technologies (ref. PF-65IN-1502) that exhibits a nominal surface resistance (provided by the supplier) of less than 10 Ω/sq and ensures good transparency in the visible spectrum (see Fig. 6), measured using a PerkinElmer Lambda 900 UV/VIS/NIR Spectrometer.

PETG is a modification of PET. The 'G' stands for glycol, which is added to PET to deliver different chemical properties. PETG ensures improved strength and durability compared to PET, and it is better suited to higher temperatures and, also, to the realization of filaments for Additive Manufacturing (AM) 3D-printing technology. Both PET and PETG are highly transparent in the visible spectrum and are particularly well-suited to be used as the substrate of transparent antennas for solar panel and space applications [13].

For the sake of simplicity, in this work, we have used 3D-printed PETG to realize the frame supporting the curved patch. In this regard, it should be noted that when PETG is employed for AM 3D-printing in its pure form (without any coloring agent), it results translucent, with a light transmittance that is strongly dependent on the printing fill density and pattern. As an example, in Fig. 6, we also report the transmittance of a 2 mm-thick 3D-printed PETG substrate with a 100% infill and an aligned rectilinear pattern (with 90° cross-hatching). This measurement is also performed using the Perkin Elmer Lambda 900 UV/VIS/NIR spectrometer but using a barium sulphate ($BaSO_4$) coated integrating sphere suitable for wavelengths between 300 and 1300 nm.

It is worth mentioning that the PETG transmittance in Fig. 6, providing a value of around 50% up to 1300 nm, has been reported by way of example only to obtain an estimation of the transmittance of 3D-printed PETG. The full characterization of this 3D-printed material is beyond the scope of this work since it depends on several 3D-printing setting parameters. Moreover, this manufacturing choice, leading to a reduced transparency of the supporting frame, is only dictated by the necessity of realizing a convenient proof of concept of the TCPA, whereas the industrial production of PET and PETG is definitely able to provide thermoplastics with higher transparency.

The dielectric permittivity of the 3D-printed PETG in the S frequency band is 2.5, and its loss tangent is 0.01. These values have been measured using the microstrip T-resonator method [25]. The dielectric permittivity of the 0.2 mm-thick PET film is assumed to be the same.

Finally, the conductivity of the In_2O_3/Au/Ag coating on the 0.2 mm-thick PET film has been estimated. Since the thickness of this coating is proprietary, we have directly measured the surface resistance to verify the exact value of our sample in the range provided by the supplier (4-10 Ω/sq). In particular, three different measurements have been performed:

i) a measurement of the static surface resistance of flat samples;
ii) a measurement of the static surface resistance of curved samples with different radius of curvature R_C and with the coating deposited on the convex surface;
iii) a measurement of the surface resistance in the S frequency band.

The results of measurements *i*) and *ii)* on the samples shown in Fig. 7 are reported in Table 4. From these results, we can observe that a radius of curvature larger than 15 mm does not affect the surface resistance.

The estimation of the surface resistance in the S frequency band has been performed by computing the return loss of an open stub of known length and width (see inset in Fig. 8) and comparing it with the return loss of the same structure

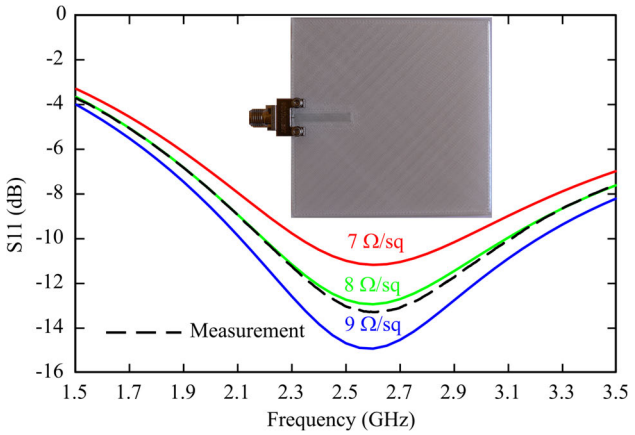

FIGURE 8. Reflection coefficient of the open stub shown in the inset. Width of the stub = 2.8 mm, Length of the stub = 20 mm.

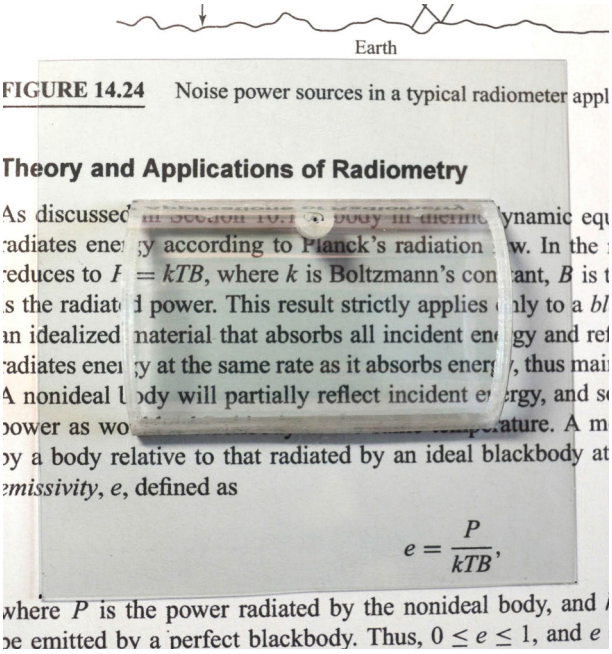

FIGURE 9. Photo of the manufactured prototype (without coaxial connector for a better evaluation of the optical transparency).

simulated using Ansys HFSS for different values of the surface resistance (see plots in Fig. 8). The best fit is achieved for a surface resistance of 8 Ω/sq.

Finally, it is worth noting that the radius of curvature $R_H = 16$ mm, selected for the antenna design in section II, preserves the static conductivity of the In2O3/Au/Ag coating (see Table 4). We assume that this bending does not affect the conductivity in the S band, as well. Therefore, the surface resistance of the TCF used for the experimental verification presented in the next section will be assumed equal to 8 Ω/sq.

IV. EXPERIMENTAL VERIFICATION

Two (virtually) identical prototypes of the curved antenna have been manufactured (see Figs. 9 and 10) to assess the electromagnetic simulations presented in Section II using the materials listed in Section III. The TCFs have been stuck on

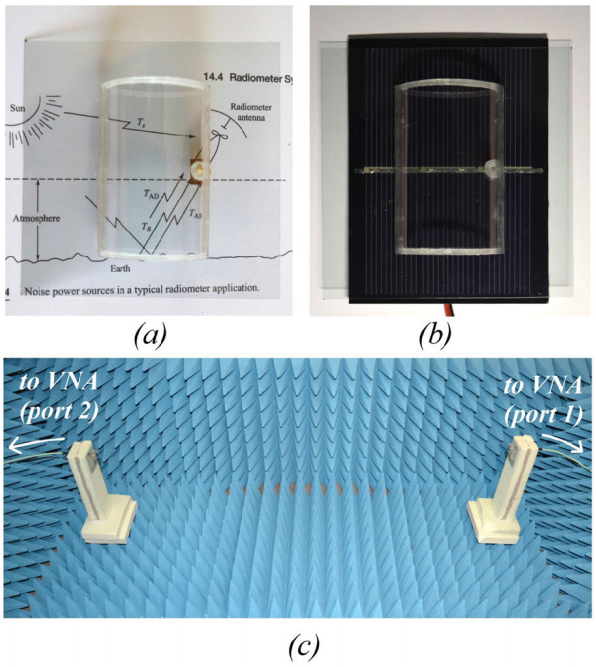

FIGURE 10. (a) Antenna under test; (b) antenna under test on a small off-the-shelf solar panel; (c) experimental set up for the measurement of the realized gain by the two-antenna method [26].

the PETG frame using a transparent non-conductive adhesive, whereas the coaxial connector has been glued to the TCFs by using a silver loaded conductive epoxy adhesive. The weight of the fabricated antenna is about 5 g and it presents a good transparency, as shown in Fig. 9, wherein the partially opaque areas are due to the 2mm-thick PETG supporting frame (having 50% transmittance, see Fig. 6). The photo in Fig. 9 depicts the antenna without coaxial connector for a better evaluation of the optical transparency and to estimate the effect of the PETG supporting frame. However, replacing the 3D-printed PETG with its counterpart from industrial production could boost the PETG transparency up to 90%-95%, thus eliminating the partially opaque areas and improving the antenna overall transparency. A photo of the complete antenna prototype, including the coaxial connector, is reported in Fig. 10a.

A. OPTICAL PERFORMANCE

The light transmittance of the proposed transparent antenna can be measured with a comparative experiment, as made in [13] and [22], by computing the ratio of the output power of a solar cell in the presence of the antenna (P_{WA}) to the output power of the solar cell in the absence of the antenna (P_{WOA}). To perform this measurement, the antenna is placed on a small off-the-shelf polycrystalline silicon solar panel of dimension 80 mm × 60 mm (Fig. 10b). To achieve a consistent estimation of the light transmission, the antenna has been arranged to cover the entire solar panel. For this experiment, the SMA connector has not been glued to the antenna to ensure a perfect fit between the antenna and the solar panel. In practical applications, the SMA can be positioned in the spaces between adjacent solar cells

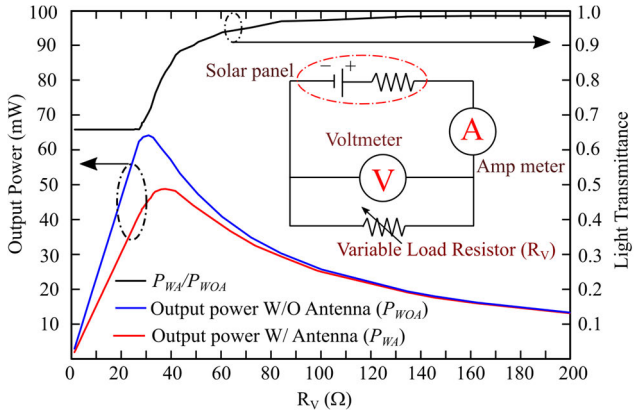

FIGURE 11. Measured output powers of the solar panel and light transmittance.

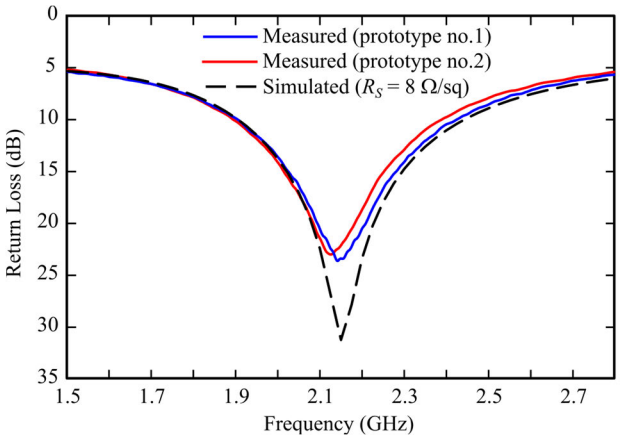

FIGURE 12. Comparison between simulated and measured return loss of the manufactured prototypes.

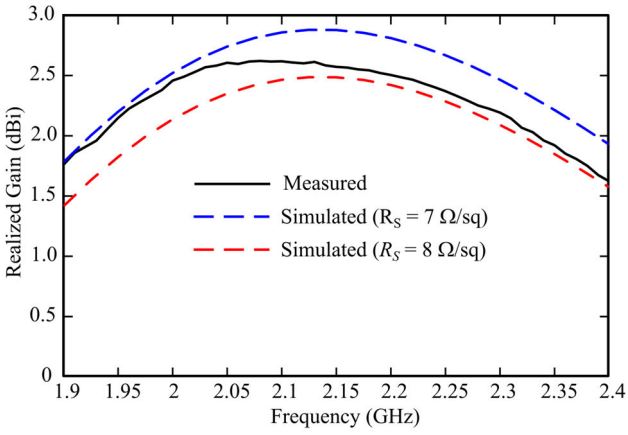

FIGURE 13. Comparison between simulated (both with $R_S = 8$ Ω/sq and $R_S = 7$ Ω/sq) and measured realized gain of the manufactured prototype.

or a via can be created in the solar panel to house the SMA connector.

The experimental setup has been housed in a dark room and a compact 14 Watt fluorescent lamp is employed as the equivalent light source. The distance between the lamp and the solar panel is set to 10 cm. The solar panel under illumination behaves as a power source and it is connected to a variable load resistor (from 1 Ω to 1000 Ω). Then, two multimeters are employed to measure the current and the voltage of the load resistor according to the equivalent circuit depicted in Fig. 11.

Based on the measured output powers, the light transmittance has been derived in Fig. 11 as P_{WA}/P_{WOA}. It can be observed that the transmittance is 71% at the peak output power of the solar panel without the antenna, and rapidly increases to above 90% as the output power decreases.

B. ELECTROMAGNETIC PERFORMANCE

The experimental verification of the electromagnetic performance has been made in an anechoic environment (Fig. 10c) by using the Anritsu MS46322B two-port vector network analyzer (VNA). The realized gain of the antenna under test (AUT) is measured by the two-antenna method (as defined in sections 8.3.1 and 8.3.2 of [26]) assuming that the two manufactured prototypes are identical.

In Fig. 12 and 13, the return loss and the realized gain of the AUT are plotted, respectively. The slight difference in the 10 dB return loss bandwidth (493/518 MHz-measured against 537 MHz-simulated) is probably due to the small uncertainty of the surface resistance of different samples of the same In_2O_3/Au/Ag coating. The agreement between simulated and measured realized gain is good as well, with a measured gain at 2.15 GHz equal to 2.57 dBi. The measured realized gain in the operating band results slightly larger than the simulated one with a surface resistance $R_S = 8$ Ω/sq. As apparent from the results in Fig. 13, where we also report the simulated gain for $R_S = 7$ Ω/sq, this suggests that the actual value of the surface resistance of the TCF sample used to manufacture the antennas could be between 7 and 8 Ω/sq. This is also consistent with the smaller bandwidth of the measured return loss over the simulated one with $R_S = 8$ Ω/sq (see Fig. 12 and Table 2).

Finally, since the bandwidth of this resonant antenna is quite large, the far-field pattern of the manufactured prototype has been measured at selected frequencies in the operating bandwidth, i.e., at 2.0 GHz, 2.15 GHz, and 2.30 GHz. The measurement setup is the same as in Fig. 10c, but one of the AUT has been placed on a rotating plate and the other one has been replaced by a test calibrated antenna (model HyperLOG 7060 by AARONIA AG), which has been connected to a broadband Low Noise Amplifier (LNA) (model ZX60-83LNS+ by Minicircuits) to improve the sensitivity of the measurement. The far-field pattern in the principal planes is reported in Fig. 14. A good agreement between measurement and simulation is observed, with a stable far-field behavior over the operating band. It is worth noting that the simulated E-plane cross-polar component is not shown because lower than -50 dB and we did not measure the back radiation due to the obstacle represented by the test coaxial cable connected to the VNA.

V. CONCLUSION AND FUTURE WORK

A curved patch antenna design has been proposed as a solution to improve the efficiency and gain of transparent

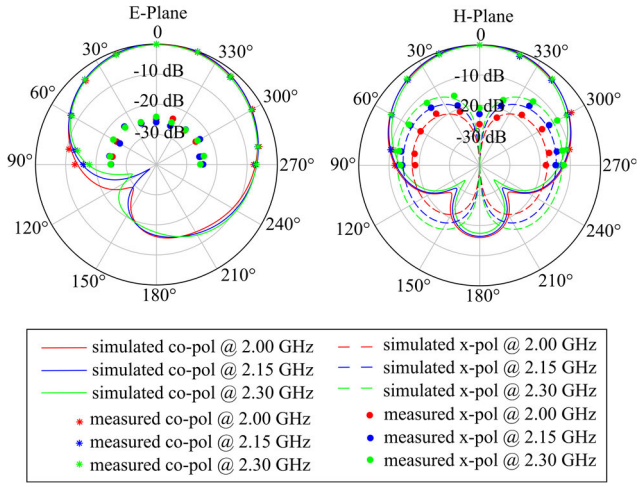

FIGURE 14. Comparison between simulated and measured normalized radiation pattern.

microstrip antennas. A transparent conductive film, deposited on a 0.2 mm-thick PET layer, is employed to implement the conductive parts and a thin frame, made of polyethylene terephthalate glycol, is used as curved support. As a result, for a surface resistance $R_S \geq 2$ Ω/sq, the simulated efficiency of the TCPA at 2.15 GHz increases by at least a factor of 4 in comparison with the transparent flat antenna. The simulated realized gain of the TCPA reaches 5.31dBi for $R_S = 2$ Ω/sq, with an improvement of 4.8 dB over the flat counterpart. It should be observed that the bandwidth of the TCPA for values of surface resistance of the TCF greater/equal than 2 Ω/sq is wide enough to cover both the uplink (2.025 - 2.11 GHz) and downlink (2.2 - 2.29 GHz) frequency bands for Telemetry, Tracking and Command applications. This feature, together with the high transparency achievable, the extremely low weight, and the compact size in the resonant direction (with a reduction of about 46% compared with the planar counterpart), makes the TCPA suitable to be used as an antenna for solar panel and satellite applications. A prototype of the designed antenna has been fabricated, using a commercially available TCF, both to assess the analysis of the electromagnetic performance and to demonstrate the feasibility of the proposed solution.

The presented curved configuration appears very promising also for a possible integration into a solar cell. In this case, the solar cell will be considered as part of the antenna substrate and the ground plane will be provided by the back-side of the solar cell, which is usually a good conductor. This solution, which will be investigated in the future, could provide improved radiation efficiency thanks to the ground plane made of a good conductor, and better transparency since it requires only one layer of TCF on the surface of the solar cell exposed to the light.

ACKNOWLEDGMENT

The authors would like to thank Paolo Pintus and Pierluigi Ortu for their useful advices, and Manuela Traversari for helping in the measurement setup.

REFERENCES

[1] Z. J. Silva, C. R. Valenta, and G. D. Durgin, "Optically transparent antennas: A survey of transparent microwave conductor performance and applications," *IEEE Antennas Propag. Mag.*, vol. 63, no. 1, pp. 27–39, Feb. 2021.
[2] G. Clasen and R. Langley, "Meshed patch antennas," *IEEE Trans. Antennas Propag.*, vol. 52, no. 6, pp. 1412–1416, Jun. 2004.
[3] T. W. Turpin and R. Baktur, "Meshed patch antennas integrated on solar cells," *IEEE Antennas Wireless Propag. Lett.*, vol. 8, pp. 693–696, 2009.
[4] T. Yasin and R. Baktur, "Circularly polarized meshed patch antenna for small satellite application," *IEEE Antennas Wireless Propag. Lett.*, vol. 12, pp. 1057–1060, 2013.
[5] T. W. Turpin and R. Baktur, "See-through microstrip antennas and their optimization," in *Proc. Gen. Assem. Int. Union Radio Sci.*, Chicago, IL, USA, Aug. 2008, pp. 1–4.
[6] X. Liu, D. R. Jackson, J. Chen, J. Liu, P. W. Fink, G. Y. Lin, and N. Neveu, "Transparent and nontransparent microstrip antennas on a CubeSat: Novel low-profile antennas for CubeSats improve mission reliability," *IEEE Antennas Propag. Mag.*, vol. 49, no. 2, pp. 59–68, Apr. 2017.
[7] N. Guan, H. Furuya, K. Himeno, K. Goto, and K. Ito, "A monopole antenna made of a transparent conductive film," in *Proc. Int. Workshop Antenna Technol., Small Smart Antennas Metamater. Appl.*, Mar. 2007, pp. 263–266.
[8] H. J. Song, T. Y. Hsu, D. F. Sievenpiper, H. P. Hsu, J. Schaffner, and E. Yasan, "A method for improving the efficiency of transparent film antennas," *IEEE Antennas Wireless Propag. Lett.*, vol. 7, pp. 753–756, 2008.
[9] T. Yasin, R. Baktur, and C. Furse, "A study on the efficiency of transparent patch antennas designed from conductive oxide films," in *Proc. IEEE Int. Symp. Antennas Propag. (APSURSI)*, Jul. 2011, pp. 3085–3087.
[10] G. Sun, B. Muneer, and Q. Zhu, "A study of microstrip antenna made of transparent ITO films," in *Proc. IEEE Antennas Propag. Soc. Int. Symp. (APSURSI)*, Jul. 2014, pp. 1867–1868.
[11] T. Peter, T. A. Rahman, S. W. Cheung, R. Nilavalan, H. F. Abutarboush, and A. Vilches, "A novel transparent UWB antenna for photovoltaic solar panel integration and RF energy harvesting," *IEEE Trans. Antennas Propag.*, vol. 62, no. 4, pp. 1844–1853, Apr. 2014.
[12] C. Kocia and S. V. Hum, "Design of an optically transparent reflectarray for solar applications using indium tin oxide," *IEEE Trans. Antennas Propag.*, vol. 64, no. 7, pp. 2884–2893, Jul. 2016.
[13] S. Zarbakhsh, M. Akbari, M. Farahani, A. Ghayekhloo, T. A. Denidni, and A. R. Sebak, "Optically transparent subarray antenna based on solar panel for CubeSat application," *IEEE Trans. Antennas Propag.*, vol. 68, no. 1, pp. 319–328, Jan. 2020.
[14] S. Hong, Y. Kim, and C. W. Jung, "Transparent microstrip patch antennas with multilayer and metal-mesh films," *IEEE Antennas Wireless Propag. Lett.*, vol. 16, pp. 772–775, 2016.
[15] P. Lippens and U. Muehlfeld, "Indium tin oxide (ITO): Sputter deposition processes," in *Handbook of Visual Display Technology*, J. Chen, W. Cranton, M. Fihn, Eds. Berlin, Germany: Springer-Verlag, 2012, pp. 779–794.
[16] E. A. Alwan, A. Kiourti, and J. L. Volakis, "Indium tin oxide film characterization at 0.1–20 GHz using coaxial probe method," *IEEE Access*, vol. 3, pp. 648–652, 2015.
[17] T. Yasin, R. Baktur, and C. Furse, "A comparative study on two types of transparent patch antennas," in *Proc. XXXth URSI Gen. Assem. Scientific Symp.*, Istanbul, Turkey, Aug. 2011.
[18] G. Muntoni, G. Montisci, G. A. Casula, F. P. Chietera, A. Michel, R. Colella, L. Catarinucci, and G. Mazzarella, "A curved 3-D printed microstrip patch antenna layout for bandwidth enhancement and size reduction," *IEEE Antennas Wireless Propag. Lett.*, vol. 19, no. 7, pp. 1118–1122, Jul. 2020.
[19] S. Abulgasem, F. Tubbal, R. Raad, P. I. Theoharis, S. Lu, and S. Iranmanesh, "Antenna designs for CubeSats: A review," *IEEE Access*, vol. 9, pp. 45289–45324, 2021.
[20] K. Lu and K. W. Leung, "On the circularly polarized parallel-plate antenna," *IEEE Trans. Antennas Propag.*, vol. 68, no. 1, pp. 3–12, Jan. 2020.
[21] A.-N. Nguyen, V. Hoang Le, N. Nguyen-Trong, M. Radfar, A. Ebrahimi, K. Phan, and A. Desai, "Dual-polarized slot antenna for full-duplex systems with high isolation," *IEEE Trans. Antennas Propag.*, vol. 69, no. 11, pp. 7119–7124, Nov. 2021.
[22] W. An, L. Xiong, S. Xu, F. Yang, H.-P. Fu, and J.-G. Ma, "A Ka-band high-efficiency transparent reflectarray antenna integrated with solar cells," *IEEE Access*, vol. 6, pp. 60843–60851, 2018.

[23] G. A. Casula, G. Montisci, and G. Mazzarella, "A wideband PET inkjet-printed antenna for UHF RFID," *IEEE Antennas Wireless Propag. Lett.*, vol. 12, pp. 1400–1403, 2013.
[24] M. Haghzadeh, C. Armiento, and A. Akyurtlu, "Microwave dielectric characterization of flexible plastic films using printed electronics," in *Proc. 87th ARFTG Microw. Meas. Conf. (ARFTG)*, May 2016, pp. 1–4.
[25] K.-P. Lätti, M. Kettunen, J.-P. Ström, and P. Silventoinen, "A review of microstrip T-resonator method in determining the dielectric properties of printed circuit board materials," *IEEE Trans. Instrum. Meas.*, vol. 56, no. 5, pp. 1845–1850, Oct. 2007.
[26] *IEEE Recommended Practice for Antenna Measurements*, IEEE Standard 149, 2021.

GIORGIO MONTISCI (Senior Member, IEEE) received the M.S. degree in electronic engineering and the Ph.D. degree in electronic engineering and computer science from the University of Cagliari, Cagliari, Italy, in 1997 and 2000, respectively. Since February 2022, he has been a Full Professor of electromagnetic fields with the University of Cagliari, teaching courses in electromagnetics and microwave engineering. He has authored or coauthored 79 papers in international journals. His current research interests include the analysis and design of waveguide slot arrays, RFID antennas, wearable antennas, numerical methods in electromagnetics, and microwave circuits and systems. He was awarded the IEEE Access Outstanding Associate Editor of 2020 and 2021. He is an Associate Editor of IEEE Access, *IET Microwaves, Antennas and Propagation*, and *IET Electronics Letters*, and an Academic Editor of the *International Journal of Antennas and Propagation*.

GIOVANNA MURA (Member, IEEE) received the M.S. degree in electronic engineering and the Ph.D. degree in electronic engineering and computer science from the University of Cagliari, Cagliari, Italy, in 2000 and 2004, respectively. Since October 2012, she has been an Assistant Professor of electronics with the University of Cagliari, teaching courses in reliability and diagnostics of electron devices. She has authored or coauthored 47 papers in international journals. Her research interests include failure physics, diagnostics of microelectronics, reliability in harsh environments (automotive and space applications), and the physical detection of counterfeit electronics. She is an Associate Editor of the *Microelectronics Reliability*, *Electronics*, *Power Electronic Devices and Components*, and *e-Prime*.

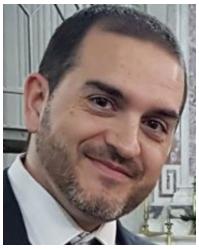

GIACOMO MUNTONI received the bachelor's degree in electronic engineering, the master's degree in telecommunication engineering, and the Ph.D. degree in electronic engineering and computer science from the University of Cagliari, Cagliari, Italy, in 2010, 2015, and 2019, respectively.

He is currently working as a Technologist with the Applied Electromagnetics Group, University of Cagliari. His research interests include design and characterization of antennas for biomedical and aerospace applications, microwave–based dielectric characterization of materials, 3-D printing of RF components, and monitoring of the space debris environment in low Earth orbit with the Sardinia Radio Telescope, in collaboration with the Cagliari Astronomical Observatory.

GIOVANNI ANDREA CASULA (Senior Member, IEEE) received the M.S. degree in electronic engineering and the Ph.D. degree in electronic engineering and computer science from the University of Cagliari, Cagliari, Italy, in 2000 and 2004, respectively.

Since December 2017, he has been an Associate Professor of electromagnetic fields with the University of Cagliari, teaching courses in electromagnetics and antenna engineering. He has authored or coauthored about 50 papers in international journals. His current research interests include the analysis and design of waveguide slot arrays, RFID antennas, wearable antennas, numerical methods in electromagnetics. He is an Associate Editor of the IEEE Transactions on Antennas and Propagation, *IET Microwaves, Antennas and Propagation*, *Electronics* (MDPI), and *Sensors* (MDPI), and an Academic Editor of the *International Journal of Antennas and Propagation*.

FRANCESCO PAOLO CHIETERA received the M.S. degree in communication engineering from the University of Salento, Lecce, Italy, in 2018, where he is currently pursuing the Ph.D. degree. His M.S. thesis named "Enhanced UHF RFID Antennas Exploiting Additive Manufacturing 3D Printing." He is currently working with the Electromagnetic Solutions for Hi-Tech (EMTech) Group, Department of Innovation Engineering, University of Salento, led by Prof. Luca Catarinucci.. He has coauthored more than 30 papers on his research topics both in international journals and conferences. His main research interests include 3-D printing in electromagnetics, RFID technologies for sensing and traceability, and the IoT applications.

MAHMOUD ABURISH-HMIDAT received the B.Sc. degree in physics from Bethlehem University, Palestine, in 1996, the master's degree in optical technologies from the AILUN Institute, and the Ph.D. degree in physics from the University of Cagliari defending a thesis on "Optical Fiber Evanescent Wave Sensors."

In 1997, he joined as a Visiting-Scientist at ICTP for training on fiber optics. In 1998, he joined the AILUN Institute in Sardinia. He have some years of experience in optical physics and photonics, mostly employed in industry. Since 2005, he has been a Technical Supervisor and the Head of quality control and thin-film coating with FILAR Optomaterials, with key responsibility in research and development, technical marketing, optics production, and process engineering. He contributes in the development of novel laser crystals for space-oriented projects such ALADIN laser transmitter (on Aeolus satellite), supervising the manufacturing and validation of laser-crystal components. His recent research interest includes the development of highly Cr-doped Alexandrite crystals for next generation high-power lasers operating in earth-observation space missions.

Open Access funding provided by 'Università degli Studi di Cagliari' within the CRUI CARE Agreement